Synthesis of Multifunctional Aza-Substituted Ruthenocene Derivatives Displaying Charge-Transfer Transitions and Selective Zn(II) Ions Sensing Properties

Francisco Otón, Arturo Espinosa, Alberto Tárraga,* and Pedro Molina*

Departamento de Química Orgánica, Facultad de Química, Universidad de Murcia, Campus de Espinardo, E-30100 Murcia, Spain

Received July 26, 2007

The synthesis, electrochemical, electronic, and cation sensing properties of multinuclear nitrogen-rich [2.2]- and [3.3]-mixed ferrocene and ruthenocene metallocenophanes are presented. Structural features of these new structural motifs are that the two redox organometallics fragments are linked by unsaturated nitrogen functionalities, for example, carbodiimide or aldimine, as well as the nitrogen atom is directly attached to the ruthenocene unit. The key bis(iminophosphorane) **3** is readily prepared by the Staudinger reaction between triphenylphosphine and 1,1′-diazidoruthenocene **2**, which has been prepared from 1,1′-dilithioruthenocene and 2,4,6-trisopropylbenzenesulfonyl azide (trisyl azide). Subsequent aza-Wittig reactions of **3** with the appropriate carbonyl or thiocarbonyl compounds provided the opened ruthenocene-based isothiocyanate **4**, and the closed carbodiimide **5** and aldimines **6** and **7**. Spectroelectrochemical studies of carbodiimide **5** and aldimine **7** revealed the presence of low-energy bands in the near-IR region in the partially oxidized forms, at 1029 and 1481 nm, respectively, which indicate the existence of intramolecular charge transfer between the iron and the ruthenium centers. The experimental data and conclusions are supported by DFT computations. Moreover, the aldimine **7** behaves as a selective colorimetric chemosensor molecules for Zn^{2+} ions. The low-energy (LE) band of the absorption spectrum of this compound is red-shifted by 99 nm, only in the presence of Zn^{2+} ions. This change in the absorption spectrum is accompanied by a dramatic color change, which allows the potential for "naked eye" detection.

Introduction

Metallocenes that have a nitrogen atom directly bonded to the five-membered ring are not very common because substitution reactions at the cyclopentadieneyl ring are not straightforward, neither with nitrogen-based nucleophiles nor with an electrophilic source of nitrogen, which are strong oxidants or relatively unstable compounds. Another drawback is the fact that aminocyclopentadienes of the type $C_5H_5NR_2$ are thermally and oxidatively rather sensitive compounds,[1] and, consequently, very few functionalized aminoferrocenes have been reported. The most general method involves the reaction of metalated ferrocenes with a nitrogen-based electrophile.[2] In this context, *o*-benzylhydroxylamine has been used with lithioferrocene to yield aminoferrocene, albeit in low yield (13%).[3] A recent optimized procedure, which allows the isolation of aminoferrocene in 50% yield, involves the use of α-azidostyrene as a source of nitrogen.[4] The synthesis of 1,1′-diazidoferrocene has been reported by reaction of 1,1′-dilithioferrocene with either 1,1,2,2-tetrabromoethane and subsequent halide displacement using $NaN_3/CuCl$[5] or 2,4,6-triisopropylbenzenesulfonyl azide (trisyl azide).[6] Diastereoselective *ortho*-metalation involving chiral ferrocenyl derivatives and trapping of the lithiated species with *N*,*O*-bis(trimethylsilyl)hydroxylamine[7] or tosyl azide[8] represents an efficient route to aminoferrocene derivatives with planar chirality.

As compared to ferrocene ligands, the ruthenocene ligands have received much less attention. Although some C-substituted[9] and heteroatom-substituted ruthenocene derivatives[10] have been reported, the chemistry of nitrogen-substituted ruthenocenes remains unexplored.

It is known that the distances between the two cyclopentadienyl rings in ferrocene and ruthenocene are 3.32 and 3.68 Å, respectively.[11] The longer distance by about 10% in ruthenocene than their ferrocene analogues would be expected to present different complexation behavior with transition metals. To date, enhanced responsiveness of a ferrocene reporter group to transition-metal ions has been achieved only by means of a family of ligands derived from amino-substituted ferrocenes, in which at least one nitrogen donor atom of a chelating ligand is directly linked to the cyclopentadienyl ring of the ferrocene unit.[12]

* To whom correspondence should be addressed. E-mail: pmolina@um.es (P.M.); atarraga@um.es (A.T.).

(1) Togni, A.; Hayashi, T. *Ferrocenes: Homogeneous Catalysis, Organic Synthesis, Material Science*; VCH: Weinheim, 1995.

(2) For a review on electrophilic amination of carbanions, see: Erdick, E.; Ay, M. *Chem. Rev.* **1989**, *89*, 1949.

(3) (a) Knox, R. G.; Pauson, P. L.; Willison, D.; Solcaniova, E.; Toma, S. *Organometallics* **1990**, *9*, 301. (b) El-Shihi, T.; Siglmüler, F.; Herrman, R.; Calvaho, M. F. N. N.; Pombeiro, A. J. L. *J. Organomet. Chem*. **1987**, *355*, 239.

(4) van Leusen, D.; Hessen, B. *Organometallics* **2001**, *20*, 224.

(5) Shafir, A.; Power, M. P.; Whitener, G. D.; Arnold, J. *Organometallics* **2000**, *19*, 3978−3982.

(6) (a) Tárraga, A.; Otón, F.; Espinosa, A.; Velasco, M. D.; Molina, P.; Evans, D. J. *Chem. Commun*. **2004**, 458. (b) Otón, F.; Espinosa, A.; Tárraga, A.; Ramirez de Arellano, C.; Molina, P. *Chem.*−*Eur. J.* **2007**, *13*, 5742.

(7) (a) Casarini, A.; Dembrach, P.; Lazzari, D.; Marini, E.; Reginato, G.; Ricci, A.; Seconi, G. *J. Org. Chem.* **1993**, *58*, 5620. (b) Riant, O.; Samuel, O.; Flessner, T.; Taudien, S.; Kagan, M. B. *J. Org. Chem.* **1997**, *62*, 6733.

(8) (a) Priego, J.; Mancheño, O. G.; Cabrera, S.; Carretero, J. C. *J. Chem. Soc., Chem. Commun.* **2001**, 2026. (b) Priego, J.; Mancheño, O. G.; Cabrera, S.; Carretero, J. C. *J. Org. Chem*. **2002**, *67*, 1346.

10.1021/om700757m CCC: $37.00
Publication on Web 10/25/2007

In a continuation of our ongoing studies involving the synthesis and structural characterization of new families of nitrogen-rich metallocenophanes with interesting structural, electrochemical, and optical properties,[6,13] we have now focused our attention on developing convenient synthetic entries to a new type of 1,1′-diazasubstituted ruthenocenes, diaza[2,2]rutenocenophanes, and an unprecedented tetraaza[3.3]ferrocenoruthenocenophane in which the two metallocene units are directly attached by carbodiimide functions.

Results and Discussion

Synthesis. The general strategy used for the synthesis of both [2,2] and [3,3] metallocenophane derivatives is based on the aza-Wittig reaction of 1,1′-bis(*N*-triphenylphosphoranylideneamino)ruthenocene derivative with the appropriate carbonyl component.

The bis(iminophosphorane) **3** is readily prepared by the Staudinger reaction between triphenylphosphine and 1,1′-diazidoruthenocene **2**, which has been prepared from ruthenocene by using 2,4,6-triisopropylbenzenesulfonyl azide (trisylazide) as a strong azide-transfer reagent. Thus, reaction of 1,1′-dilithioruthenocene with trisylazide at 0 °C afforded directly **2**, which could be isolated as a pure but unstable solid in 35% yield. Reaction of **2** with triphenylphosphine in CH_2Cl_2 at room temperature provided the bis(iminophosphorane) **3** in 95%. Nevertheless, compound **2** could be used, without further purification, for the next step in the Staudinger reaction with triphenylphosphine, which allows the one-flask conversion of ruthenocene **1** into the bis(iminophosphorane) **3** in an overall yield of 74%.[14]

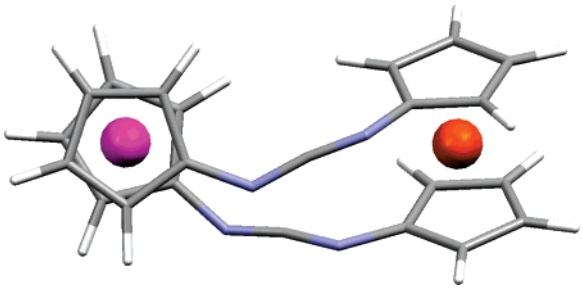

Figure 1. Calculated (B3LYP/6-31G*/Lanl2DZ-ecp) structure for the most stable conformer $\mathbf{5}_{C1}$.

Interestingly, the aza-Wittig reaction of **3** with 1,1′-diisocyanatoferrocene[15] resulted in the final bis(carbodiimide) **5** (72%), with an unprecedented tetraza[3,3](1,1′)ferrocenoruthenocenophane structure. On the other hand, the reaction between the bis(iminophosphorane) **3** and carbon disulfide gave the 1,1′-diisothiocyanatoruthenocene **4** in 41% yield.[16] We have found two conformational minima for this compound **5** by means of DFT-based theoretical calculations: the absolute minimum in the Gibbs free energy surface has no symmetry ($\mathbf{5}_{C1}$) (Figure 1) and can be converted into a 1.40 kcal/mol less stable C_2-symmetric conformer ($\mathbf{5}_{C2}$) (see the Supporting Information). In the most stable conformer $\mathbf{5}_{C1}$, the intermetallic Ru···Fe distance is 6.525 Å with both metallocenes twisted by 56.0° from each other (angle between axes connecting Cp ring centroids in each metallocene), whereas in the $\mathbf{5}_{C1}$ isomer both metallocenes are almost orthogonal (twisting angle 78.5°) bringing closer both metal centers (6.395 Å). Frequency analysis of $\mathbf{5}_{C1}$ reveals two characteristic normal vibration modes corresponding to the asymmetric and quasi-symmetric coupled stretching of both carbodiimide moieties (2190 and 2150 cm^{-1}, respectively; scaling factor 0.9656), in perfect agreement with the experimental values (2190 and 2125 cm^{-1}). All attempts to prepare the [3,3](1,1′)diruthenocenophane analogous to **5**, by the aza-Wittig reaction between the ruthenocene derivatives bis(iminophosphorane) **3** and the 1,1′-diisothiocyanatoruthenocene **4**, were totally unsuccessful.

The new structural motifs diaza[2,2]homometallocenophane **6** and heterometallocenophane **7** were prepared, in 63% and 42% yield, respectively, by aza-Wittig reaction of the bis(iminophosphorane) **3** and the appropriate 1,1′-diformylmetallocene as carbonyl partners (Scheme 1). By contrast, the isomeric heterobimetallic metallocenophane **9** was prepared in 59% yield by aza-Wittig reaction between the bis(iminophosphorane) **8**[6] and 1,1′-diformylruthenocene, which was easily prepared by dilithiation of ruthenocene and subsequent reaction with dimethylformamide as the electrophile, following a modification of a previously described procedure.[9k] For all three diaza[2,2]dimetallocenophanes **6**, **7**, and **9**, our DFT-based calculations predict the occurrence of C_2-symmetric absolute minima and slightly less stable *quasi*-C_s-symmetric conformers ($\Delta G°_{C2/qCs}$ 0.57, 0.12, and 1.36 kcal/mol, respectively) (see the Supporting Information).

(9) Ethenes: (a) Sato, M.; Kudo, A.; Kawata, Y.; Saitoh, H. *Chem. Commun.* **1996**, 25. (b) Sato, M.; Kawata, Y.; Kudo, A.; Saitoh, H.; Ochiai, S. *J. Chem. Soc., Dalton Trans.* **1998**, 2215. (c) Sato, M.; Nagata, T.; Tanemura, A.; Fujihara, T.; Kumakura, S.; Untura, K. *Chem.—Eur. J.* **2004**, *10*, 2166. (d) Obendorf, D.; Schottenberger, H.; Wurst, K.; Schuler, N.; Laus, G. *J. Organomet. Chem*. **2005**, *690*, 811. Ethynes: (e) Sato, M.; Watanabe, M. *Chem. Commun*. **2002**, 1574. (f) Sato, M.; Kubota, Y.; Kawata, Y.; Fujihara, T.; Unoura, K.; Oyama, A. *Chem.—Eur. J.* **2006**, *12*, 2282. Aryl(heteroaryl): (g) Bolm, C.; Hermanns, N.; Kesselgruber, M.; Hildebrand, J. P. *J. Organomet. Chem.* **2001**, *624*, 157. (h) Sato, M.; Maruyama, G.; Tanemura, A. *J. Organomet. Chem*. **2002**, *655*, 23. (i) Enders, M.; Kohl, G.; Pritzkow, H. *Organometallics* **2002**, *21*, 1111. (j) Sato, M.; Kubota, Y.; Tanemura, A.; Maruyama, G.; Fujihara, T.; Nakayama, J.; Takayanagi, T.; Takahashi, K.; Unoura, K. *Eur. J. Inorg. Chem.* **2006**, 4577. Carbonyl derivatives: (k) Sanders, R.; Mueller-Westerhoff, U. T. *J. Organomet. Chem*. **1996**, *512*, 219. (l) Sato, M.; Suzuki, M.; Okoshi, M.; Kurasina, M.; Watanabe, M. *J. Organomet. Chem*. **2002**, *648*, 72. (m) Sanderson, C. T.; Quinian, J. A.; Conover, R. C.; Johnson, M. K.; Murphy, M.; Dluhy, R. A.; Kutal, C. *Inorg. Chem.* **2005**, *44*, 3283. (n) Cooke, M. W.; Cameron, T. S.; Robertson, K. N.; Swarts, J. C.; Aquino, M. A. S. *Organometallics* **2002**, *21*, 5962.

(10) Borane derivatives: (a) Appel, A.; Nörth, H.; Schmidt, M. *Chem. Ber*. **1995**, *128*, 621. (b) Wrackmeyer, B.; Dörfler, U.; Milius, W.; Heberhold, M. *Polyhedron* **1995**, *14*, 1425. Phosphorous derivatives: (c) Li, S.; Wei, B.; Low, P. M. N.; Lee, H. K.; Hor, T. S. A.; Xue, F.; Mak, T. C. W. *J. Chem. Soc., Dalton Trans.* **1997**, 1289. (d) Liu, D.; Xie, F.; Zhang, W. *Tetrahedron Lett.* **2007**, *48*, 585.

(11) (a) Dunitz, J.; Orgel, L.; Rich, A. *Acta Crystallogr*. **1956**, *9*, 373. (b) Hardgrove, G.; Templeton, D. *Acta Crystallogr*. **1959**, *12*, 28.

(12) (a) Plenio, H.; Burth, D. *Organometallics* **1996**, *15*, 4054. (b) Gibson, V. C.; Long, N. J.; Marshall, E. L.; Oxford, P. J.; White, A. J. P.; Williams, D. J. *J. Chem. Soc., Dalton Trans*. **2001**, 1162. (c) Shafir, A.; Fiedler, D.; Arnold, J. *J. Chem. Soc., Dalton Trans*. **2002**, 555. (d) Shafir, A.; Fiedler, D.; Arnold, J. *Chem. Commun*. **2003**, 2598. (e) Gibson, V. C.; Halliwell, C. M.; Long, N. J.; Oxford, P. J.; Smith, A. M.; White, A. J. P.; Williams, D. J. *Dalton Trans.* **2003**, 918. (f) Weng, Z.; Koh, L. L.; Hor, T. S. A. *J. Organomet. Chem.* **2004**, *689*, 18.

(13) (a) Tarraga, A.; Molina, P.; Lopez, J. L.; Velasco, M. D.; Bautista, D. *Organometallics* **2002**, *21*, 2055. (b) Lopez, J. L.; Tarraga, A.; Espinosa A.; Velasco, M. D.; Molina, P.; Lloveras, V.; Vidal-Gancedo, J.; Rovira, C.; Veciana, J.; Evans, D. J.; Wurst, K. *Chem.-Eur. J*. **2004**, *10*, 1815. (c) Caballero, A.; Lloveras, V.; Tarraga, A.; Espinosa, A.; Velasco, M. D.; Vidal-Gancedo, J.; Rovira, C.; Wurst, K.; Molina, P.; Veciana, J. *Angew. Chem., Int. Ed.* **2005**, *44*, 1977. (d) Otón, F.; Tarraga, A.; Espinosa, A.; Velasco, M. D.; Bautista, D.; Molina, P. *J. Org. Chem.* **2005**, *70*, 6603. (e) Caballero, A.; Garcia, R.; Espinosa, A.; Tarraga, A.; Molina, P. *J. Org. Chem.* **2007**, *72*, 1161.

(14) For a review of bis(iminophosphoranes), see: Arques, A.; Molina, P. *Curr. Org. Chem*. **2004**, *8*, 827.

(15) Petrovitch, P. M. *Double Liaison* **1996**, *133*, 1093. Petrovitch, P. M. *Chem. Abstr*. **1968**, *68*, 29843s.

(16) For work dealing with the synthesis of isothiocyanates from iminophosphoranes and carbon disulfide, see: Molina, P.; Alajarin, M.; Arques, A. *Synthesis* 1**982**, 596.

Scheme 1. Synthesis of 1,1′-Disubstituted Ruthenocene Derivatives 2−4 and 10, and Ruthenocenophanes 5−7 and 9[a]

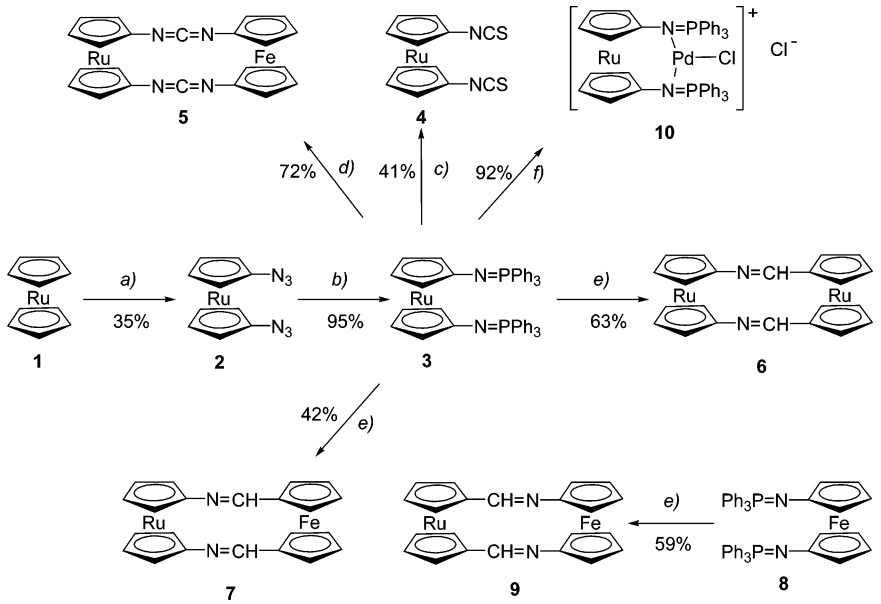

[a] Reagents: (a) (i) *n*-BuLi, TMEDA, Et_2O, rt; (ii) 2,4,6-triisopropylphenylsulfonylazide, 0 °C; (b) PPh_3, CH_2Cl_2, rt; (c) CS_2, 45 °C; (d) 1,1′-bisisocyanatoferrocene, dry THF, rt; (e) 1,1′-diformylruthenocene, toluene, reflux; (f) dichlorobis(acetonitrile)palladium(II), toluene, rt.

The structures of the ruthenocenophane compounds and the other ruthenocene derivatives prepared were determined by means of standard spectroscopic techniques (IR, ^{1}H and ^{13}C NMR), mass spectrometry, and elemental analyses, all data being in agreement with the proposed structures.

The signals observed in the ^{1}H NMR spectra of the [3,3] and [2,2] ferrocenoruthenocenophanes are informative for the structural elucidation of these compounds and were assigned on the basis of the analogy to that of the corresponding [3,3]-ferrocenophane previously described[6] and by using COSY experiments. In general, the NMR spectra of these metallocenophanes show four signals, with the appearance of pseudo-triplets and with a proton ratio of 1:1:1:1, which are in good agreement with two A_2B_2 systems typical of monosubstituted cyclopentadiene rings. The analysis of the ^{1}H NMR corresponding to both [2,2]ferrocenoruthenocenophanes also revealed the following general facts: (i) Hα and Hβ present in the Cp ring of the metallocene directly linked to the aldimine carbon atom are deshielded with respect to the corresponding Hα' and Hβ' present in the Cp ring of the metallocene directly linked to the nitrogen atom of the imine bridge; (ii) Hα and Hα' are deshielded as compared to Hβ and Hβ'; (iii) Hα are deshielded with respect to Hα'; and (iv) Hβ are deshielded with respect to Hβ', except in compound **7**. It should be underlined that ^{13}C NMR spectra of diaza[2,2]ruthenocenophane **6** could not be recorded because of its low solubility. However, its HR-EI mass spectrum displays an intense isotopic cluster peaking at *m*/*z* 512.95658 assignable to the molecular ion. The relative abundance of the isotopic cluster is in good agreement with the simulated spectrum.

The behavior of ruthenocenyl bisiminophosphorane **3** as homobidentate ligand for palladium metal cation was also studied. Thus, reaction of iminophosphorane **3** with dichlorobis-(acetonitrile)palladium(II) in toluene gave the corresponding dichloro palladium(II) complex **10**, which was characterized spectroscopically. Notably, a remarkable downfield shift was observed in its ^{31}P NMR spectrum (δ 35.8 ppm) when compared to the free iminophosphorane **3** (δ 7.9 ppm), which indicates the partial positive character of the phosphorus atom in the complex. Moreover, the ^{1}H NMR spectrum of **10** afforded the α- and β-ring protons of the ruthenocene moiety as two broad singlets downshifted (+1.36 ppm) at δ 5.41 and upshifted (−0.09 ppm) at δ 3.67 ppm, respectively. Consequently, the difference in the chemical shift of the monosubstituted cyclopentadienyl ring protons is higher in complex **10** ($\Delta\delta$ = 1.74 ppm) than in the free ligand **3** ($\Delta\delta$ = 0.29 ppm). A two-dimensional ^{1}H−^{13}C correlation experiment (HMQC) verified the coherence of two ^{13}C signals at 77.9 (Cβ) and 72.5 (Cα) ppm with the signals at 5.41 and 3.67 ppm, respectively, in the ^{1}H NMR spectrum. The precise structure of compound **10** is unknown due to our inability to obtain single crystals for X-ray analysis. Nevertheless, several structural features can be established from the spectral and X-ray data corresponding to several related ferrocenyl palladium complexes already reported.[17] In such cases, a difference in chemical shifts of the signals corresponding to the hydrogen atoms of the cyclopentadienyl rings, of approximately 2 ppm, is indicated that constitutes a strong evidence of a trans coordination. Additionally, the X-ray analysis of some of those complexes also revealed that the Pd center was cationic and nearly square planar with the nitrogen atoms in a pseudo-trans coordination geometry, which favored the formation of a dative Fe−Pd bond. On the basis of the analogy of **10** to the above-mentioned ferrocenyl palladium complexes, we can then assume the same kind of trans coordination and the possible presence of a dative Ru−Pd bond in this new ruthenocenyl palladium complex **10**. The presence of three phenyl rings on each phosphorus atom may restrict the electron donation to the nitrogen atoms through resonance, thus leaving the Pd(II) center electronically unsaturated and favoring the formation of a dative bond Ru−Pd. The FAB$^+$ mass

(17) (a) Mann, G.; Shelby, Q.; Roy, A. H.; Hartwig, J. F. *Organometallics* **2003**, *22*, 2775. (b) van Leeuwen, P. W. N. M.; Zuideveld, M. A.; Swennenhuis, B. H. G.; Freixa, Z.; Kamer, P. C. J.; Goubitz, K.; Fraanje, J.; Lutz, M.; Spek, A. L. *J. Am. Chem. Soc.* **2003**, *125*, 5523. (c) Seyferth, D.; Hames, B. W.; Rucker, T. G.; Cowie, M.; Dickson, R. S. *Organometallics* **1983**, *2*, 472. (d) Fillion, E.; Taylor, N. J. *J. Am. Chem. Soc.* **2003**, *125*, 12700. (e) Akabori, S.; Kumagai, T.; Shirahige T.; Sato, S.; Kawazoe, K.; Tamura, C.; Sato, M. *Organometallics* **1987**, *6*, 526. (f) Akabori, S.; Kumagai, T.; Shirahige T.; Sato, S.; Kawazoe, K.; Tamura, C.; Sato, M. *Organometallics* **1987**, *6*, 2105. (g) Metallinos, C.; Tremblay, D.; Barret, F. B.; Taylor, N. J. *J. Organomet. Chem.* **2006**, *691*, 2044.

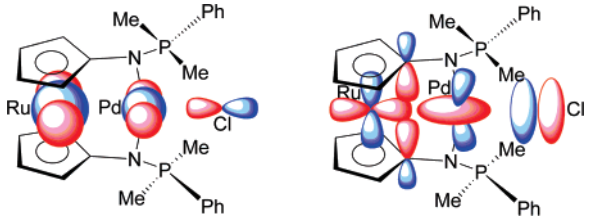

Figure 2. HOMO−4 (left) and HOMO−6 (right) simplified representation for the calculated (B3LYP/6-31G*/Lanl2DZ-ecp) structure of model complex **10′**.

spectrum of **10** shows a peak at *m*/*e* 923, corresponding to $M^+ - {}^{35}Cl$. The nature of this bidentate ruthenocene, in which the coordinating heteroatoms are nitrogen atoms, is also supported by conductivity measurements[18] carried out in acetone solutions of complex **10** ($c = 2.5 \times 10^{-4}$ M). The calculated molar conductivity was $\Lambda_M = 99.28$ cm^2/Ω·mol, which is within the range typical for a 1:1 electrolyte. The proposed structural features for **10** are in agreement with the calculated (B3LYP/6-31G*/Lanl2DZ-ecp) geometry for the C_2-symmetric bis(dimethylphenylphosphoranilidene) analogue **10′** (Figure 2) that shows the Pd atom in a nearly perfect square-planar environment (angles N−Pd−N 162.3°) with a rather small Ru−Pd distance (2.799 Å). This suggests some kind of Ru−Pd bond, which is confirmed by the NBO (Natural Bond Orbital) analysis that indicates a moderate bonding interaction (WBI_{Ru-Pd} 0.193) when compared to those of both Ru and Pd with their respective neighbors ($WBI_{Ru-C(Cp)}$ 0.285 average; WBI_{Pd-N} 0.298; WBI_{Pd-Cl} 0.362). This bonding interaction is clearly observed in molecular orbitals HOMO−4 and HOMO−6 sketched in Figure 2. Also, using the Bader's AIM (Atoms-In-Molecules) methodology,[19] through a topological analysis of the electronic charge density $\rho(r)$ a bond critical point (3,−1) has been found within the Ru−Pd axis (the so-called bond path) at 1.382 Å from the later, having $\rho(r_c) = 6.22 \times 10^{-3}$ e/Å^3 and $\nabla^2\rho(r_c) = 3.18 \times 10^{-3}$ e/Å^5. Moreover, the gas-phase calculated variation in chemical shift was $\Delta\delta^P_{calc} = +43.7$ ppm when moving from the model 1,1′-bis(dimethylphenylphosforanilidenamino)ruthenocene free ligand **3′** to the corresponding model complex **10′**, in reasonable agreement with the experimentally obtained value ($\Delta\delta^P_{exper} = +27.9$ ppm).

Electrochemical and Optical Properties. Electrochemical studies using cyclic voltammetry (CV) and Osteryoung square wave voltammetry (OSWV), at room temperature, were performed to evaluate the different redox entities present in the new metallocene and metallocenophane derivatives prepared.

The CV response of **3** in CH_2Cl_2, also containing 0.1 M [*n*-Bu_4N]PF_6 as supporting electrolyte, showed an electrochemically reversible one-electron oxidation process at $E_{1/2} = -0.58$ V versus ferrocene/ferrocenium (Fc/Fc^+) redox couple ($\Delta E = E_{pc} - E_{pa} = 85$ mV) (see the Supporting Information). This value is higher than that required to oxidize the ferrocene unit in the related 1,1′-bis(triphenylphosphoranilidenamino)ferrocene ($E_{1/2} = -0.84$ V).[6a] In both cases, the large cathodic shifts observed for their $E_{1/2}$, when compared to the redox potentials of other ferrocene and ruthenocene derivatives, are consistent with the high degree of electron donation from the iminophosphorane groups. Likewise, the OSWV voltammogram also exhibits an oxidation peak at formal potential of −0.58 V vs Fc/Fc^+. The electrochemical behavior of this ruthenocene derivative is rather unusual because it is well known that

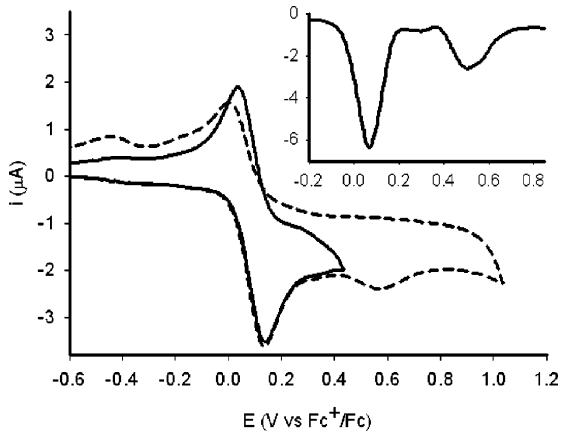

Figure 3. Cyclic voltammogram of compound **5** (1×10^{-3} M) in CH_2Cl_2 using [(*n*-$Bu)_4N$]PF_6 (0.1 M) as supporting electrolyte, scanned at 0.2 V s^{-1} from −0.6 to 0.4 V (solid line) and from −0.6 to 1.0 V (dashed line). Inset: OSWV of compound **5** (1×10^{-3} M) in CH_2Cl_2 using [(*n*-$Bu)_4N$]PF_6 (0.1 M) as supporting electrolyte, scanned at 0.1 V s^{-1} from −0.2 to 0.8 V.

ruthenocene and its derivatives, as opposed to their ferrocene analogues, usually undergo an irreversible one-step two-electron oxidation process.[20] The reasons given for this behavior are either a rapid dimerization of the ruthenocenium (Cp_2Ru^+) species that is generated followed by disproportionation or the direct disproportionation of (Cp_2Ru^+), in the presence of weakly coordinating ligands. A quasi-reversible one-electron oxidation of ruthenocene derivatives has only been observed in molten salts,[21] in noncoordinating solvent using a noncoordinating electrolyte,[22] or by introducing steric hindrance around the metal by completely methylating the Cp rings to form Cp^*_2Ru species.[23]

The CV of the tetraza[3,3]ferrocenoruthenocenophane **5**, in CH_2Cl_2, displays two one-electron oxidation waves (Figure 3). The first one corresponds to a reversible oxidation process at 0.08 V vs Fc/Fc^+ ($\Delta E = E_{pc} - E_{pa} = 100$ mV) and arises from the oxidation of the ferrocene unit. The second wave of the CV appears at $E_p = 0.54$ V and is associated with an irreversible oxidation of the ruthenocene unit. The OSWV voltammogram also exhibits two oxidation peaks at formal potentials of 0.08 and 0.52 V vs Fc/Fc^+, respectively.

The CV of the isomeric diaza[2,2]heterobimethallocenophanes **7** and **9** shows two oxidative processes. In compound **7**, a first one-electron reversible oxidation wave appears at $E_{1/2} = 0.16$ V vs Fc/Fc^+ redox couple ($\Delta E = E_{pc} - E_{pa} = 84$ mV), while the second one, at $E_p = 0.52$ V, is associated with an irreversible oxidative process (see the Supporting Information). Similarly, the isomeric metallocenophane **9** also exhibits a reversible oxidation wave at $E_{1/2} = -0.08$ V vs Fc/Fc^+ redox couple ($\Delta E = E_{pc} - E_{pa} = 80$ mV) and a second irreversible oxidation process ($E_p = 0.77$ V vs Fc/Fc^+) (Figure 4). The CV for the diaza[2,2]ruthenocenophane **6** could not be carried out due to the very low solubility of this compound.

The UV/vis spectra of heterobimetallocenophanes **5**, **7**, and **9** could be explained on the basis of the individual ferrocene

(18) Geary, W. J. *Coord. Chem. Rev.* **1971**, *7*, 81.
(19) Bader, R. F. W. *Atoms in Molecules: A Quantum Theory*; Oxford University Press: Oxford, 1990.
(20) (a) Kuwana, T.; Bublitz, D. E.; Hoh, G. *J. Am. Chem. Soc.* **1960**, *82*, 5811. (b) Gubin, S. P.; Smirnova, L. I.; Denisovich, L. I.; Lubovich, A. A. *J. Organomet. Chem.* **1971**, *30*, 243. (c) Denisovich, L. I.; Zakurin, N. V.; Bazrukova, A. A.; Gubin, S. P. *J. Organomet. Chem.* **1974**, *81*, 207.
(21) Gale, R. J.; Job, R. *Inorg. Chem.* **1981**, *20*, 42.
(22) Hill, M. G.; Lamanna, W. M.; Mann, K. R. *Inorg. Chem.* **1991**, *30*, 4687.
(23) (a) Koelle, U.; Salzer, A. *J. Organomet. Chem.* **1983**, *243*, C27. (b) Koelle, U.; Grub, J. *J. Organomet. Chem.* **1985**, *289*, 133.

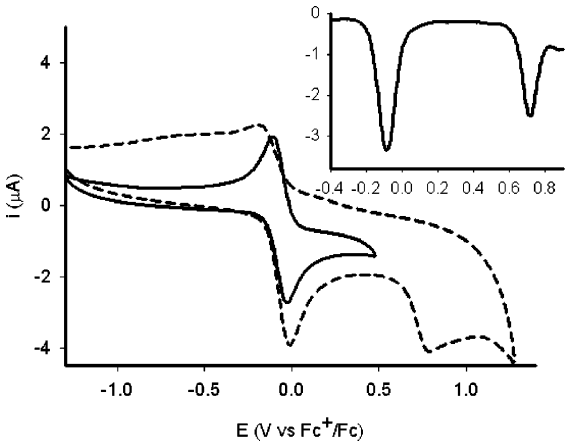

Figure 4. Cyclic voltammogram of compound **9** (1×10^{-3} M) in CH_2Cl_2 using $[(n\text{-Bu})_4N]PF_6$ (0.1 M) as supporting electrolyte, scanned at 0.2 V s^{-1} from −1.5 to 0.5 V (solid line) and from −1.5 to 1.5 V (dashed line). Inset: OSWV of compound **9** (1×10^{-3} M) in CH_2Cl_2 using $[(n\text{-Bu})_4N]PF_6$ (0.1 M) as supporting electrolyte, scanned at 0.1 V s^{-1} from −0.4 to 1.0 V.

and ruthenocene components of each dyad (see the Supporting Information). Thus, the UV/vis spectrum of tetraza[3,3]ferrocenoruthenocenophane **5** is characterized by an intense ligand-centered absorption band at 260 nm along with an absorption band at 356 nm, which is ascribed to a Ru^{II}-to-ligand (MLCT) transition.[24] In addition, another weaker low-energy (LE) absorption band is visible at 488 nm, which is produced either by nearly degenerate transitions, an Fe^{II} d−d transition,[23] or by a Fe^{II}-to-ligand (MLCT) process ($d_{\pi-\pi^*}$).[25] Similar UV/vis spectra are exhibited by the diaza[2,2]ferrocenophaneruthenocenophanes **7** and **9** (see the Supporting Information).

Spectroelectrochemistry. To study the electronic interaction between the two metallocene subunits present in compounds **5**, **7**, and **9**, spectrophotometric studies were carried out on their electrochemically generated oxidized derivatives. Generation of the oxidized species derived from **5** was performed by constant potential electrolysis, 0.12 V above the $E_{1/2}$ of the ferrocenyl redox couple (0.20 V), and monitored by absorption spectroscopy. Interestingly, during the oxidation process, a new weak and broad band grew in the near-IR region at $\lambda_{max} = 1029$ nm ($\epsilon_{max} = 1470$ M^{-1} cm^{-1}), reaching its maximum after complete formation of $\mathbf{5}^{\bullet+}$ (Table 1) (Figure 5). As in the CV, the first redox wave (0.08 V) was assigned to the one-electron process occurring at the Fe center ($Fe^{II/III}$); this new absorption band (1029 nm) can be attributed to the metal−metal charge transfer (MMCT) from Ru^{II} to Fe^{III} sites. The intensity of this band subsequently decreases until it disappears when the dication $\mathbf{5}^{2+}$ is completely formed.

To compare the magnitude of the electronic communication between the two metallocene subunits present in this heterobinuclear system **5** and the previously reported tetraaza[3,3]-ferrocenophane **11**[6a] (Chart 1), we have now carried out the same spectroelectrochemical study on this derivative.

It was already described[6a] that compound **11** displays two reversible one-electron oxidation waves at a formal potential of +0.09 and +0.29 V vs Fc^+/Fc. Thus, the generation of the monooxidized species derived from this homobimetallic derivative **11** was performed by constant potential electrolysis at 0.21 V. During the oxidation ($0 \le n \le 1$), the band observed in compound **11** at $\lambda = 440$ nm progressively disappears, and at the same time a new and weak absorption band appears in the near-IR region, at $\lambda = 1395$ nm ($\epsilon = 101$ M^{-1} cm^{-1}), whose intensity continuously increases until one electron is removed, and which is assigned to an intervalence charge transfer (IVCT) from the Fe^{II} to Fe^{III} sites (Table 1). Along with the changes of these bands, a defined isosbestic point at $\lambda = 773$ nm is maintained during the course of the oxidation process. On removing two electrons ($1 \le n \le 2$) at the constant potential of 0.41 V, the intensity of this band decreases until it disappears when the dioxidized $\mathbf{11}^{2+}$ species is completely formed (see the Supporting Information).

TD-DFT (time-dependent DFT) calculations performed on the optimized structures for $\mathbf{5}^{\bullet+}$ and $\mathbf{11}^{\bullet+}$ (see the Supporting Information) showed the expected transitions in the near-IR region (unscaled values 1194.0 and 1225.3 nm, respectively), which were attributed to optical excitations from a filled β-MO mainly located on the reduced metal center (β-HOMO of

Table 1. UV−Visible/Near-IR Data in CH_2Cl_2

compd	λ_{max} [nm] (10^{-3} ϵ [M^{-1} cm^{-1}])
5	260 (sh), 334 (sh), 434 (0.48)
$\mathbf{5}^{\bullet+}$ [a]	241 (sh), 273 (23.28), 402 (sh), 478 (1.93), 590 (1.83), 1029[b] (1.47)
$\mathbf{5}^{2+}$ [a]	277 (sh), 416 (2.59), 589 (sh)
7	260 (18.10), 351 (5.16), 497 (sh)
$\mathbf{7}^{\bullet+}$ [a]	262 (18.82), 349 (sh), 406 (2.32), 557 (sh), 1481[b] (0.95)
$\mathbf{7}^{2+}$ [a]	265 (13.14), 290 (13.82), 347 (4.34), 421 (3.53)
11	265 (32.70), 338 (sh), 440 (1.46)
$\mathbf{11}^{\bullet+}$ [a]	274 (48.32), 432 (4.88), 609 (sh), 843 (0.63), 1395[b] (1.01)
$\mathbf{11}^{2+}$ [a]	406 (11.08), 573 (sh), 859 (4.66)

[a] Oxidized species obtained electrochemically in CH_2Cl_2 (5×10^{-4} M) using $[n\text{-Bu}_4N][PF_6]$ (0.15 M) as supporting electrolyte. [b] Values obtained by deconvolution of the experimental spectra.

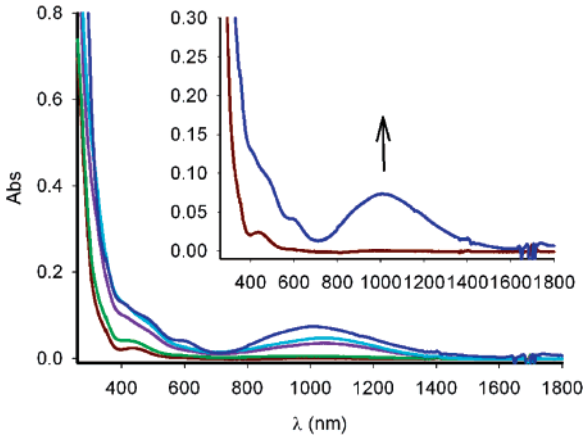

Figure 5. Evolution of the UV−vis−NIR spectra during the course of the oxidation of compound **5** (5×10^{-4} M) in CH_2Cl_2 with $[(n\text{-Bu})_4N]PF_6$ (0.15 M) as supporting electrolyte when 1 electron is removed. Arrow indicates absorptions that increase during the experiment.

Chart 1

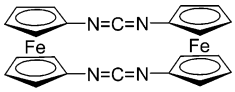

11

(24) (a) Sohn, Y. S.; Hendrickson, D. N.; Gray, M. B. *J. Am. Chem. Soc.* **1971**, *93*, 3603. (b) Sanderson, C. T.; Quinian, J. A.; Conover, R. C.; Johnson, M. K.; Murphy, M.; Dluhy, R. A.; Kuntal, C. *Inorg. Chem.* **2005**, *44*, 3283. (c) Gao, L.-B.; Zhang, L.-Y.; Shi, L.-X.; Cheng, Z.-N. *Organometallics* **2005**, *24*, 1678.

(25) Barlow, S.; Bunting, H. E.; Ringham, C.; Green, J. C.; Bublitz, G. U.; Boxer, S. G.; Perry, J. W.; Marder, S. R. *J. Am. Chem. Soc.* **1999**, *121*, 3715.

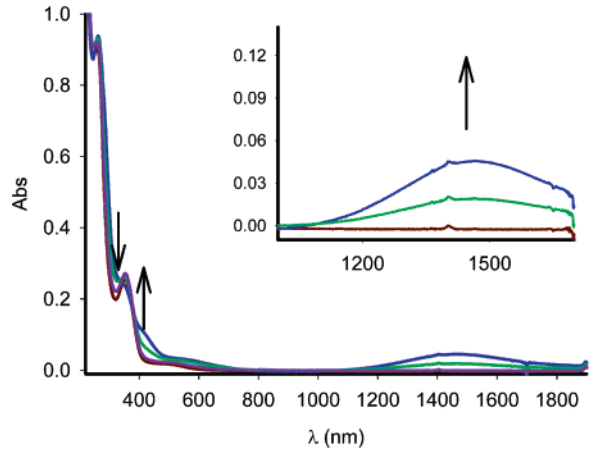

Figure 6. Evolution of the UV−vis−NIR spectra during the course of the oxidation of compound **7** (5×10^{-4} M) in CH_2Cl_2 with $[(n\text{-}Bu)_4N]PF_6$ (0.15 M) as supporting electrolyte when 1 electron is removed. Arrows indicate absorptions that increase during the experiment.

Ru-$d_{x^2-y^2}$-type in $\mathbf{5}^{\bullet+}$) to the β-LUMO mainly consisting of a $d_{x^2-y^2}$-type AO centered at the oxidized Fe atom.

Previous reports have emphasized that spectral measurements of the IVCT transitions often serve as a very accurate probe for the degree of electronic coupling.[26a]The spectral parameters of the bands present in the near-IR, energy (ν_{max}), intensity (ϵ_{max}), and half-bandwidth ($\Delta\nu_{1/2}$), obtained by deconvolution of the experimental spectra performed on spectral intensity times wavenumber versus wavenumber assuming Gaussian shapes, have been used to determine the effective electronic coupling (V_{ab}) through the two-state classical Marcus−Hush theory.[26]

According to Robin and Day classification,[26b] mixed-valence compounds are classified in three categories: class I, where the redox centers are completely localized and behave as separate entities; class II, where an intermediate coupling between the mixed-valence centers exists; and class III, where the system is completely delocalized and the redox centers show intermediate valence states.

For the class II regime, the $\Delta\nu_{1/2theo}$ and the electronic coupling V_{ab} are derived from the Hush equations $\Delta\nu_{1/2theo} = (2310\nu_{max})^{1/2}$ and $V_{ab} = (0.0205/d_{ab})(\epsilon_{max}\nu_{max}\Delta\nu_{1/2})^{1/2}$, where d_{ab} is the diabatic metal−metal distance (i.e., the intermetallic distance in the hypothetical absence of electronic coupling). Additionally, the delocalization coefficient α, which is a parameter that quantifies the degree of valence delocalization in the ground state (i.e., the fraction of valence electronic charge transferred from the donor to the acceptor metal centers), can be calculated by using the equation $\alpha = V_{ab}/\nu_{max}$.[27] Taking into account this consideration, the values of $V_{ab} = 493$ cm^{-1} and $\alpha = 0.069$ were calculated for compound $\mathbf{11}^{\bullet+}$, which are quite similar to those obtained for the heterobimetallic system $\mathbf{5}^{\bullet+}$: $V_{ab} = 651$ cm^{-1} and $\alpha = 0.067$.

Likewise, generation of the monooxidized species derived from the [2,2]ferrocenoruthenocenophane **7** was performed by constant potential electrolysis, 0.12 V above $E_{1/2}$ of the ferrocenyl redox couple (Figure 6). During the oxidation process, a new band, in the near-IR region, appears at $\lambda_{max} = 1481$ nm ($\epsilon_{max} = 955$ M^{-1} cm^{-1}), whose intensity continuously increases until one electron is removed, and which is also assigned to the metal−metal charge transfer (MMCT) from the Ru^{II} to Fe^{III} centers. On removing two electrons, at a constant potential of 0.64 V, the intensity of the band at $\lambda_{max} = 1481$ nm decreases until it disappears when the compound is fully oxidized. This MMCT band also agrees with our TD-DFT calculations performed on the optimized structure for $\mathbf{7}^{\bullet+}$ that predicts the occurrence of a β-HOMO → β-LUMO transition (mainly of type Ru^{II}-$d_{x^2-y^2}$ → Fe^{III}-$d_{x^2-y^2}$) (see the Supporting Information) at an unscaled wavelength of 1381.9 nm, together with another near-IR transition, not observed experimentally, at 1097.1 nm.

The application of the two-state Hush[26] model to the spectrum of the mixed-valence compounds $\mathbf{7}^{\bullet+}$ predicts a half-height bandwidth [$\Delta\nu_{1/2} = (2310l)^{1/2}$] in the case where the two redox sites are inequivalent[28] of 3721 cm^{-1}, which was larger than the value determined experimentally (2194 cm^{-1}) by spectral deconvolution assuming a Gaussian profile (see the Supporting Information). The origin of this discrepancy is not immediately clear, although differences between theoretical and experimental values of $\Delta\nu_{1/2}$ are not uncommon. They often arise from system nonidealities with respect to the model.[29] The availability of E_{MMCT} in $\mathbf{7}^{\bullet+}$ also enables the estimation of the $V_{ab} = 406$ cm^{-1} and the related ground-state delocalization coefficient $\alpha = 0.060$.

All attempts to promote a controlled oxidation process in the [2,2]ferrocenoruthenocenophane **9** failed. Thus, the full oxidized compound was only obtained, $\mathbf{9}^{2+}$, which, in turn, did not display any NIR absorption band.

Metal Ion Sensing Properties. Previous studies on ferrocene-based ligands have shown that bands ascribed to the lowest energy metal−ligand transitions, in the absorption spectra, are perturbed upon complexation.[30] Therefore, the metal recognition properties of the aza-bridged metallocene dyads **7** and **9** toward Li^+, Na^+, K^+, Ca^{2+}, Mg^{2+}, Zn^{2+}, Cd^{2+}, Hg^{2+}, Ni^{2+}, and Pb^{2+} metal ions (as their perchlorate salts) were evaluated by UV−vis spectroscopy. Titration experiments for CH_3CN/CH_2Cl_2 (3/2) solutions of these ligands ($c = 1 \times 10^{-4}$ M) and the corresponding ions were performed and analyzed quantitatively.[31] No changes were observed in the UV−vis spectra upon addition of Li^+, Na^+, K^+, Ca^{2+}, Mg^{2+}, Hg^{2+}, Ni^{2+}, and Pb^{2+} even in a large excess to the CH_3CN/CH_2Cl_2 (3/2) solutions of any of these ligands. However, significant spectrophotometric changes in the metal−ligand absorption bands were observed upon addition of increasing amounts of Zn^{2+} metal ions. In both cases, the most prominent features observed during the com-

(26) (a) Hush, N. S. *Prog. Inorg. Chem.* **1967**, *8*, 391. (b) Robin, M. B.; Day, P. *Adv. Inorg. Chem. Radiochem.* **1967**, *10*, 247. (c) Creutz, C. *Prog. Inorg. Chem.* **1983**, *30*, 1. (d) Nelsen, S. F. *Chem.—Eur. J.* **2000**, *6*, 581.

(27) (a) Barlow, S. *Inorg. Chem.* **2001**, *40*, 7047. (b) Santi, S.; Orian, L.; Durante, C.; Bisello, A.; Benetollo, F.; Crociani, L.; Ganis, P.; Ceccon, A. *Chem.-Eur. J.* **2007**, *13*, 1955.

(28) Hush theory indicates that, for a mixed-valence system with two inequivalent redox centers, the energy of the IVTC transition is given by $\tilde{\nu}_{max} = \lambda + \Delta G_0$, where λ_{max} is the reorganization energy of Marcus theory and ΔG_0 can be estimated from the electrochemical data. If one assumes that the oxidation potential of one center is unaffected by the oxidation state of the other, the magnitude of ΔG_0 is obtained by converting the electrochemical value of $\Delta E_{1/2}$ into energy units. For an elegant application, see: Barlow, S. *Inorg. Chem.* **2001**, *40*, 7047−7053.

(29) (a) Elliot, C. M.; Derr, D. L.; Matyushov, D. V.; Newton, M. D. *J. Am. Chem. Soc.* **1998**, *120*, 11714. (b) Curtis, J. C.; Meyer, T. J. *Inorg. Chem.* **1982**, *21*, 1562.

(30) (a) Marder, S. R.; Perry, J. W.; Tiemann, B. G. *Organometallics* **1991**, *10*, 1896−1901. (b) Coe, B. J.; Jones, C. J.; McCleverty, J. A.; Bloor, D.; Cross, G. J. *J. Organomet. Chem.* **1994**, *464*, 225−232. (c) Müller, T. J.; Netz, A.; Ansorge, M. *Organometallics* **1999**, *18*, 5066−5074. (d) Carr, J. D.; Coles, S. J.; Hassan, M. B.; Hurthouse, M. B.; Malik, K. M. A.; Tucker, J. H. R. *J. Chem. Soc., Dalton Trans.* **1999**, 57.

(31) Specfit/32 Global Analysis System, 1999−2004 Spectrum Software Associates (SpecSoft@compuserve.com). The Specfit program was acquired from Bio-logic, SA (www.bio-logic.info), in January 2005. The equation to be adjusted by non-linear regression, using the above mentioned software, was: $\Delta A/b = \{K_{11}\Delta\epsilon_{HG}[H]_{tot}[G]\}/\{1 + K_{11}[G]\}$, where H = host, G = guest, HG = complex, ΔA = variation in the absorption, b = cell width, K_{11} = association constant for a 1:1 model, and $\Delta\epsilon_{HG}$ = variation of molar absorptivity.

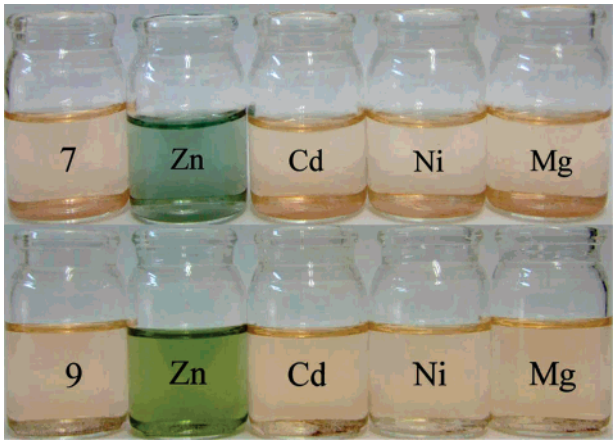

Figure 7. Color changes in CH_3CN/CH_2Cl_2 solutions of compounds **7** and **9** upon addition of several metal cations tested.

Table 2. UV−Vis Data of the Free Ligands 7 and 9 and the Corresponding Ligand/Zn^{2+} Complexes

compd	λ_{max} [nm] (10^{-3} ϵ [M^{-1} cm^{-1}])
7	230 (25.11), 261 (24.50), 350 (7.05), 496 (0.54)
7·Zn^{2+}	234 (18.78), 263 (22.69), 383 (sh), 595 (1.28)
9	260 (20.99), 356 (3.80), 488 (0.52)
9·Zn^{2+}	267 (20.87), 362 (sh), 416 (2.73), 588 (1.13)

plexation processes are the following: (i) a progressive red-shift of the corresponding metal−ligand transition band; (ii) appearance of well-defined isosbestic points, indicative of the presence of only two absorbing species in the solution the free ligand (L) and the complex (L·Zn^{2+}); and (iii) a neat change of the color during the complexation event, from pale red to deep green, which can be used for the "naked eye" detection of this divalent cation (Figure 7).

Thus, addition of increasing amounts of a solution of Zn^{2+} in CH_3CN ($c = 2.5 \times 10^{-2}$ M) to a solution of **7** in CH_3CN/CH_2Cl_2 (3/2) ($c = 1 \times 10^{-4}$ M) caused a progressive appearance of a new more intense band located at $\lambda = 595$ nm ($\epsilon = 1280$ M^{-1} cm^{-1}) as well as the complete disappearance of the initial LE band at $\lambda = 496$ nm ($\epsilon = 540$ M^{-1} cm^{-1}) (Table 2 and Figure 8). Two well-defined isosbestic points at $\lambda = 340$ and 375 nm were found, indicating that a neat interconversion

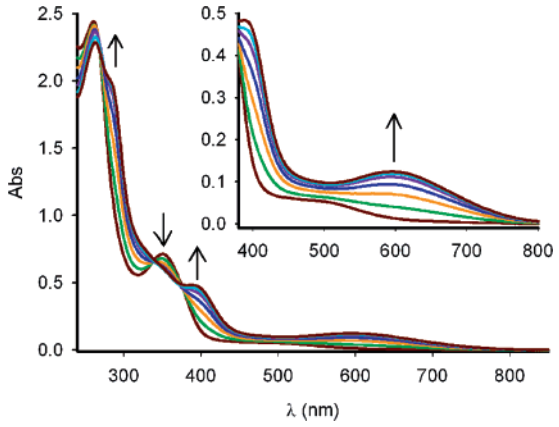

Figure 8. Changes in the absorption spectra of compound **7** [$c = 10^{-4}$ M in CH_3CN/CH_2Cl_2 (3:2, v:v)] upon addition of increasing amounts of Zn^{2+}. Arrows indicate absorptions that increase during the experiment.

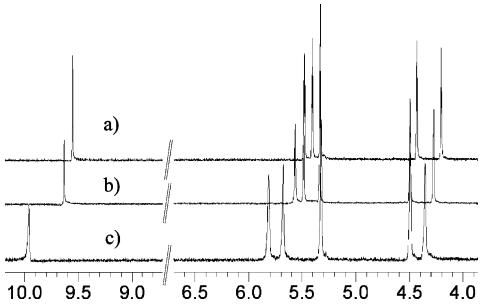

Figure 9. Evolution of the ^1H NMR spectra of **7** in CD_2Cl_2 when (a) 0 equiv, (b) 0.4 equiv, and (c) 1 equiv of $Zn(ClO_4)_2$ was added.

between the uncomplexed and complexed species occurs. The new band is red-shifted by $\Delta\lambda = 99$ nm and is responsible for the change of color from pale red (neutral ligand **7**) to deep green (complexed **7**·Zn^{2+}). The resulting titration data suggest a 2:1 (L:Zn^{2+}) binding model, with the association constant and detection limit[32] being 1.2×10^8 M^{-2} (error <10%) and 5.8×10^{-6} M, respectively.

Similarly, when ligand **9** was studied under the above-mentioned titration conditions, a significant red-shift ($\Delta\lambda = 100$ nm) of the LE band, appearing at $\lambda = 488$ nm ($\epsilon = 520$ M^{-1} cm^{-1}), was observed (Table 1), which completely disappears when the complexation was completed (see the Supporting Information). Three isosbestic points were also found during the titration process at $\lambda = 264$, 346, and 381 nm. The resulting titration fitted to a 2:1 (L:Zn^{2+}) binding model, with the association constant and detection limit being 9.3×10^6 M^{-2} (error <10%) and 6.0×10^{-6} M, respectively.

To get first-hand information about the coordinating sites of receptors **7** and **9** upon complexation, ^1H NMR experiments were performed to explore the complexation mechanism with Zn^{2+} metal ions. Thus, addition of 1 equiv of $Zn(ClO_4)_2$ in CD_3CN to a solution of the ligand **7** in CD_2Cl_2 gives rise to significant downfield shifts for the signals corresponding to the iminic proton (C*H*═N) at $\delta = 10.05$ ($\Delta\delta = +0.44$) as well as for the signals of the Hα and Hα′ ($\Delta\delta = +0.42$ and $\Delta\delta = +0.35$ ppm, respectively) and Hβ and Hβ' ($\Delta\delta = +0.23$ and $\Delta\delta = +0.11$ ppm, respectively) protons present in the Cp rings of the ferrocene and ruthenocene moieties (Figure 9). Similarly, ^1H NMR titration studies carried out by addition of 1 equiv of Zn^{2+} to a solution of the ligand **9** under the same conditions also cause downfield shifts analogous to those mentioned for ligand **7** (see the Supporting Information).

For the reported constants to be taken with confidence, we have proved the reversibility of the complexation process by carrying out the following experimental test: 0.5 equiv of $Zn(ClO_4)_2$ was added to a solution of the appropriate ligand (**7** or **9**) in CH_2Cl_2 to obtain the complexed L_2·Zn^{2+} species, whose DPV voltammogram and UV/vis spectrum were recorded. The CH_2Cl_2 solutions of the complexes were washed several times with water until the color of the solution changed from deep green to red. The organic layers were dried, the corresponding optical spectrum, DPV voltammogram, and ^1H NMR spectrum were recorded, and they were found to be the same as those of the corresponding free receptor L. Afterward, 0.5 equiv of $Zn(ClO_4)_2$ was added to each of these solutions, and the initial UV/vis spectrum, OSWV voltammogram, and ^1H NMR spectrum of the complexes L_2·Zn^{2+} were fully recovered together with its deep red color. These experiments were carried out over several cycles, and the optical spectra were recorded after each

(32) Shortreed, M.; Kopelman, R.; Kuhn, M.; Hoyland, B. *Anal. Chem.* **1996**, *68*, 1414.

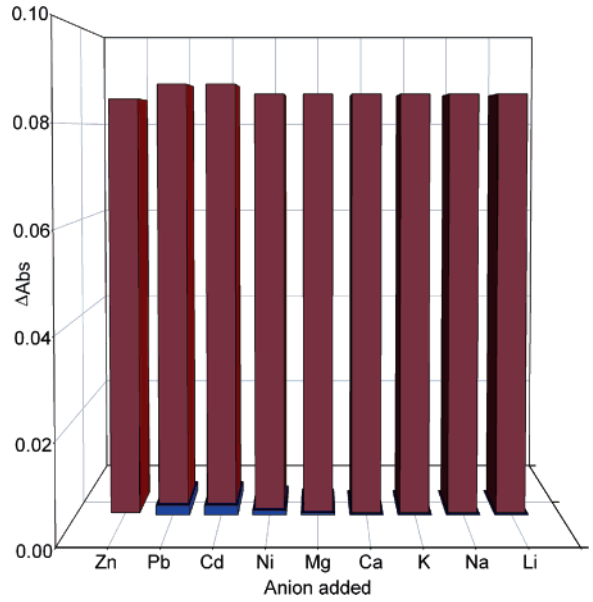

Figure 10. Bar diagram showing the results of the cross-selectivity experiments of **7** in CH_3CN/CH_2Cl_2 (3/2) upon addition of the metal tested. Blue bars indicate the absorbance increase of ligand **7** after addition of 1 equiv of the corresponding metal cation. Red bars indicate the absorbance increase of ligand **7** after addition of 0.5 equiv of Zn^{2+} to the above-mentioned (ligand+metal cation) solutions.

step and found to be fully recovered on completion of the step, thus demonstrating the high degree of reversibility of the complexation/decomplexation processes.

The interference in the selective response of ligands **7** and **9** in the presence of Zn^{2+} metal ions, from the other metal cations tested, was also studied by using cross-selectivity experiments. Thus, addition of 1 equiv of Li^+, Na^+, K^+, Ca^{2+}, Mg^{2+}, Hg^{2+}, Ni^{2+}, and Pb^{2+} cations in CH_3CN to 1 equiv of the receptors **7** and **9** in CH_3CN/CH_2Cl_2 (3/2) did not give any optical response. However, further addition of 0.5 equiv of Zn^{2+} to the above-mentioned solutions gave optical response identical to that observed upon addition of 0.5 equiv of Zn^{2+} to a solution containing only 1 equiv of the appropriate ligand and which is free of the other metal cations (see Figure 10 and the Supporting Information). These results clearly demonstrate that these receptors have excellent affinity for Zn^{2+} over those ions.

The demand for sensing Zn^{2+} metal ions, which is spectroscopically silent because of its $3d^{10}4s^0$ electronic configuration, in competitive media such as Ca^{2+} and Mg^{2+} is growing rapidly.[33] A challenge to develop chemosensors that can discriminate Zn^{2+} from Cd^{2+} is still more important. Because cadmium and zinc are in the same group of the periodic table and have similar properties, they usually cause similar spectral changes after interactions with chemosensors. In this sense, a few colorimetric selective Zn^{2+} chemosensors have been designed and synthesized.[34]

Conclusion

The synthesis, electrochemical, electronic, and optical properties of the new structural motifs nitrogen-rich [2.2]- and [3.3]-mixed ferrocene and ruthenocene metallocenophanes, bearing a nitrogen functionality (carbodiimide **5**; aldimine **6**,**7**) directly attached to the ruthenocene unit, are presented. Introduction of the nitrogen functionality into the ruthenocene unit is achieved by reaction of 1,1′-dilithioruthenocene with 2,4,6-trisopropylbenzenesulfonyl azide (trisyl azide), and the resulting 1,1′-diazidoruthenocene **2** is converted into the key bis(iminophosphorane) **3** by Staudinger reaction with triphenylphosphine. Subsequent aza-Wittig reactions of **3** with carbon disulfide provided the opened ruthenocene-based isothiocyanate **4**, whereas the reaction with 1,1′-bis(isocyanato)ferrocene afforded the closed biscarbodiimide **5**. When the appropriate 1,1′-diformylmetallocene is used, the corresponding bisaldimines **6** and **7** are obtained. These aza-substituted ruthenocene derivatives comprise remarkable multifunctional molecular systems, because they could serve as important models for the investigation of intramolecular charge transfer and for metal recognition processes. Mixed ferrocene ruthenocenophanes **5** and **7** form the mixed-valence species $\mathbf{5}^{\bullet+}$ and $\mathbf{7}^{\bullet+}$ by partial oxidation. Interestingly, the spectroelectrochemical study of the mixed metallocene **5** revealed the presence of a LE band in the near-IR region, which indicates an unprecedented intramolecular charge transfer between the ferrocene and ruthenocene units through carbodiimide bridges. On the other hand, mixed diaza[2.2]ferrocenoruthenocenophanes **7** and **9** exhibit interesting cation-sensing properties, which show high selectivity for Zn^{2+} ions. The metal−ligand transition band of the absorption spectra of these compounds is red-shifted by about 100 nm only in the presence of Zn^{2+} ions. This change in the absorption spectra is accompanied by a dramatic color change from pale red to deep green, which allows the potential for "naked eye" highly selective detection over some others cations, including the strong competitor Cd^{2+}. Unfortunately, this sensing behavior could not be studied in water solutions due to the poor solubility of these ligands in aqueous environments.

Experimental Section

Preparation of 1,1′-Bis(azido)ruthenocene 2. To a solution of ruthenocene (1 g, 4.32 mmol) in freshly distilled dry diethyl ether (18 mL) were added *n*-BuLi (6.7 mL, 10.8 mmol) and *N*,*N*,*N*,*N*-tetramethylethylendiamine (TMEDA) (1.63 mL, 10.8 mmol) under nitrogen. The solution was stirred for 18 h at room temperature, and then a solution of 2,4,6-triisopropylphenylsulfonylazide (trisyl azide) (3.9 g, 15.8 mmol) in the same solvent (15 mL) was added at 0 °C. The mixture was stirred in the dark and at room temperature for 4 h. Afterward, 30 mL of H_2O was added, and the mixture was extracted with 100 mL of diethyl ether. The organic phase was dried with anhydrous $MgSO_4$ and chromatographed on a silica gel column, using *n*-Hex/AcOEt (19:1) (R_f = 0.65) as eluent to give the corresponding azide, which was crystallized from *n*-Hex at −40 °C. Yield: 35%. Mp: 60−63 °C (dec). ^{1}H NMR (300 MHz): δ 4.83 (st, 4H, CH−Ru), 4.53 (st, 4H, CH−Ru). ^{13}C NMR (75.3 MHz): δ 102.3 (q-Cp−Ru), 68.8 (CH−Ru), 64.9 (CH−Ru). FT-IR (Nujol): ν 2117, 1290, 1163, 1061, 1026, 935, 813, 737. MS (FAB$^+$): *m*/*e* (%) 314 (M^+ + 1, 8). Anal. Calcd for $C_{10}H_8N_6Ru$: C, 38.34; H, 2.57; N, 26.83. Found: C, 38.54; H, 2.85; N, 26.62.

Preparation of 1,1′-Bis(*N*-triphenylphosphoranilidenamino)-ruthenocene 3. Method A: To a solution of ruthenocene (1 g, 4.32 mmol) in freshly distilled dry diethyl ether (18 mL) were added *n*-BuLi (6.7 mL, 10.8 mmol) and TMEDA (1.63 mL, 10.8 mmol) under nitrogen. The solution was stirred at room temperature for 18 h, and then a solution of trisyl azide (3.9 g, 15.8 mmol) in the same solvent (15 mL) was added at 0 °C. The reaction mixture

(33) (a) Valeur, B.; Leray, I. *Coord. Chem. Rev.* **2000**, *205*, 3. (b) Prodi, L.; Bolleta, F.; Montalti, M.; Zaccheroni, N. *Coord. Chem. Rev.* **2000**, *205*, 59. (c) Jiang, P.; Guo, Z. *Coord. Chem. Rev.* **2004**, *248*, 205. (d) Kikuchi, K.; Komatsu, K.; Nagano, T. *Curr. Opin. Chem. Biol.* **2004**, *8*, 182.

(34) (a) Xu, Z.; Qian, X.; Cui, J.; Zhang, R. *Tetrahedron* **2006**, *62*, 10117. (b) Zhang, L.; Dong, S.; Zhu, L. *Chem. Commun.* **2007**, 1891. (c) Zapata, F.; Caballero, A.; Espinosa, A.; Tarraga, A.; Molina, P. *Org. Lett.* **2007**, *9*, 2385.

was stirred at room temperature for 4 h and protected from light. Subsequently, H_2O (30 mL) was added, and the mixture was extracted with diethyl ether (100 mL). The organic layers were dried with anhydrous $MgSO_4$, and the solvent was removed under vacuum. The resulting solid was dissolved in dry CH_2Cl_2 (30 mL), and a solution of triphenylphosphine (2.26 g, 8.64 mmol) in the same solvent (20 mL) was added. Next, the reaction mixture was stirred for 5 h at room temperature, and afterward the solvent was reduced to 5 mL under vacuum. To this solution was added diethyl ether (30 mL), giving rise to the bisiminophosphorane **3** in 74% yield, which was used without further purification for the next step in the aza-Wittig reactions.

Method B: To a solution of 1,1′-bis(azido)ruthenocene (0.5 g, 2.16 mmol) in dry THF (30 mL) was added a solution of triphenylphosphine (1.69 g, 6.48 mmol) in the same solvent (15 mL). The reaction mixture was stirred at room temperature for 5 h, and then the solvent was reduced to 5 mL under vacuum. After addition of diethyl ether (30 mL), a solid was obtained, which was crystallized from CH_2Cl_2/diethyl ether (5:2) at −40 °C. Yield: 95%. Mp: 195−198 °C (dec). ^{1}H NMR (300 MHz): δ 7.69−7.76 (m, 12H, Ph), 7.39−7.49 (m, 18H, Ph), 4.05 (bs, 4H, CH−Ru), 3.76 (bs, 4H, CH−Ru). ^{13}C NMR (75.3 MHz): δ 132.9 (d, J = 9.7 Hz, CH_{meta}−Ph), 131.4 (d, J = 2.7 Hz, CH_{para}−Ph), 130.6 (d, J = 97.0 Hz, C_{ipso}−Ph), 128.3 (d, J = 11.8, CH_{orto}−Ph), 77.2 (q-Cp−Ru), 66.8 (CH−Ru), 66.6 (CH−Ru). ^{31}P NMR (162 MHz): δ 7.9. FT-IR (Nujol): ν 1459, 1285, 1111, 1076, 1001, 822, 787, 753, 738, 693. MS (FAB$^+$): *m*/*e* 782 (M^+ + 1, 100). Anal. Calcd for $C_{46}H_{38}N_2P_2Ru$: C, 70.67; H, 4.90; N, 3.58. Found: C, 70.42; H, 5.18; N, 3.79.

Preparation of 1,1′-Bis(isothiocyanate)ruthenocene 4. A solution of 1,1′-bis(*N*-triphenylphosphoranylidenamino)ruthenocene **3** (0.2 g, 0.26 mmol) in carbon disulfide (16 mL) was heated at 45 °C under nitrogen for 4 h, and then the solvent was removed under reduced pressure. The resulting residue was treated with diethyl ether, giving rise to a precipitate of triphenylphosphine sulfide, which was separated by filtration. The remaining solution was chromatographed on a silica gel column, using *n*-Hex/EtAcO (19:1) (R_f = 0.3), and the solid obtained, after removing the solvent, was crystallized from *n*-Hex at −40 °C. Yield: 41%. Mp: 112−113 °C. ^{1}H NMR (200 MHz): δ 4.94 (st, 4H, CH−Ru), 4.56 (st, 4H, CH−Ru). ^{13}C NMR (50 MHz): δ 89.0 (q-Cp−Ru), 70.4 (CH−Ru), 70.1 (CH−Ru). FT-IR (Nujol): ν 2101, 2060, 1312, 1209, 1163, 1106, 1029, 8.28, 724. MS (FAB$^+$): *m*/*e* (%) 346 (M^+ + 1, 7). Anal. Calcd for $C_{12}H_8N_2RuS_2$: C, 41.73; H, 2.33; N, 8.11. Found: C, 41.97; H, 2.12; N, 8.28.

Preparation of 1,3,10,12-Tetraaza-[3,3](1,1′)ferrocenoruthenocenophane 5. To a solution of 1,1′-bis(isocyanate)ferrocene[1] (0.08 g., 0.30 mmol) in dry THF (20 mL) was added a solution of 1,1′-bis(*N*-triphenilphosphoranylidenamino)ruthenocene **4** (0.155 g., 0.30 mmol) in the same solvent (40 mL). The reaction mixture was stirred at room temperature for 1 h, and the solvent was removed under vacuum. The brown solid obtained was then crystallized from CH_2Cl_2 at −40 °C. Yield: 72%. Mp: 190−193 °C (dec). ^{1}H NMR (400 MHz): δ 4.85 (st, 4H, CH−Ru), 4.52 (st, 4H, CH−Ru), 4.22 (st, 4H, CH−Fc), 4.16 (st, 4H, CH−Fc). ^{13}C NMR (100 MHz): δ 134.7 (q, carbodiimide), 97.0 (q-Cp−Ru), 95.4 (q-Cp−Fc), 68.9 (2×CH−Ru), 66.4 (CH−Fc), 66.3 (CH−Fc). FT-IR (Nujol): ν 2190, 2125, 1533, 1349, 1230, 1205, 1026, 917, 812, 728. MS (FAB$^+$): *m*/*e* 494 (M^+ + 1, 6). Anal. Calcd for $C_{22}H_{16}FeN_4Ru$: C, 53.56; H, 3.27; N, 11.36. Found: C, 53.83; H, 3.43; N, 11.09.

General Procedure for the Preparation of Diaza[2,2](1,1′)-homo- and Heterometallocenophanes 6, 7, and 9. A solution of the appropriate 1,1′-bis(*N*-triphenylphosphoranylidenamino)-metallocene **3** or **8** (0.35 mmol) and the adequate 1,1′-diformylmetallocene (0.35 mmol) in dry toluene (20 mL) was heated under reflux for 10 h under nitrogen. Subsequently, the solution was concentrated under vacuum until 5 mL, and then 5 mL of diethyl ether was added to precipitate **6** and **7** as orange solids, which were washed with CH_2Cl_2 and crystallized from CH_2Cl_2/diethyl ether. Isolation of compound **9** was achieved directly from the reaction mixture by chromatography using a silica gel column and CH_2Cl_2/MeOH (9:1) as solvent (R_f = 0.45), and further recrystallization from CH_2Cl_2 yielded the title compound as purple crystals.

6. Yield: 63%. Mp: 229−232 °C (dec). ^{1}H NMR (200 MHz): δ 9.63 (s, 2H, imine), 5.64 (st, 4H, CH−Ru), 5.38 (st, 4H, CH−Ru), 4.49 (st, 4H, CH−Ru), 4.28 (st, 4H, CH−Ru). ^{13}C NMR: good quality spectrum could not be recorded due to the very low solubility of this compound. FT-IR (Nujol): ν 1613, 1319, 1226, 1194, 1153, 1035, 1020, 954, 923, 856, 804, 723. MS (high-resolution EI$^+$): *m*/*e* (%) 512.95658 (M^+, 100). Anal. Calcd for $C_{22}H_{18}N_2Ru_2$: C, 51.55; H, 3.54; N, 5.47. Found: C, 51.79; H, 3.36; N, 5.75.

7. Yield: 42%. Mp: 238−241 °C (dec). ^{1}H NMR (400 MHz): δ 9.58 (s, 2H, imine), 5.49 (st, 4H, Cp−Fc), 5.38 (st, 4H, Cp−Ru), 4.42 (st, 4H, CH−Ru), 4.18 (st, 4H, CH−Fc). ^{13}C NMR (100 MHz): δ 168.5 (CH−imine), 104.3 (q-Cp−Ru), 81.4 (q-Cp−Fc), 70.0 (CH−Fe), 69.7 (CH−Fc), 69.4 (CH−Fc), 67.4 (CH−Fc). FT-IR (Nujol): ν 1614, 1321, 1228, 1195, 1151, 1090, 1022, 925, 873, 790. MS (FAB$^+$): *m*/*e* 469 (M^+ + 1, 78). Anal. Calcd for $C_{22}H_{18}FeN_2Ru$: C, 56.54; H, 3.88; N, 5.99. Found: C, 56.32; H, 3.70; N, 5.71.

9. Yield: 59%. Mp: 145−148 °C. ^{1}H NMR (200 MHz): δ 9.31 (s, 2H, imine), 5.68 (st, 4H, CH−Ru), 5.14 (st, 4H, CH−Fc), 4.67 (st, 4H, CH−Ru), 4.09 (st, 4H, CH−Fc). ^{13}C NMR (100 MHz): δ 162.8 (imine), 103.5 (q-Cp−Fc), 84.1 (q-Cp−Ru), 72.9 (CH−Ru), 71.9 (CH−Ru), 67.1 (CH−Fc), 64.7 (CH−Fc). FT-IR (Nujol): ν 1633, 1313, 1294, 1182, 1160, 1106, 995, 875, 748. MS (FAB$^+$): *m*/*e* 469 (M^+ + 1, 100). Anal. Calcd for $C_{22}H_{18}FeN_2Ru$: C, 56.54; H, 3.88; N, 5.99. Found: C, 56.77; H, 3.62; N, 6.27.

[1,1′-Bis(triphenylphosphoranilidenamino)ruthenocene Pd(II)Cl]Cl 10. Yield: 92%. Mp: 249−252 °C (dec). ^{1}H NMR (300 MHz): δ 7.69−7.76 (m, 12H, Ph), 7.60−7.65 (m, 6H, Ph), 7.45−7.51 (m, 12H, Ph), 5.41 (bs, 4H, CH−Ru), 3.67 (bs, 4H, CH−Ru). ^{13}C NMR (75 MHz): δ 133.5 (d, J = 10.3 Hz, CH_{meta}−Ph), 133.3 (s, CH_{para}−Ph), 128.9 (d, J = 13 Hz, CH_{orto}−Ph), 125.9 (d, J = 101.9 Hz, q-Ph), 96.5 (d, J = 16.5 Hz, q-Cp−Ru), 77.9 (s, CHβ−Ru), 72.5 (d, J = 5.5 Hz, CHα−Ru). ^{31}P NMR (121 MHz): δ 35.84. FT-IR (Nujol): ν 3090, 3048, 1435, 1366, 1310, 1287, 1186, 1158, 1114, 1075, 1058, 1029, 999, 974, 883, 824, 783, 749, 728, 692. MS (FAB$^+$): *m*/*e* (%) 923 (M^+ − ^{35}Cl, 93), 887 (M^+ − 2 ^{35}Cl, 57), 816 (M^+ − PdCl, 85), 781 (M^+ − $PdCl_2$, 51). Anal. Calcd for $C_{46}H_{38}Cl_2N_2P_2PdRu$: C, 57.60; H, 3.99; N, 2.92. Found: C, 57.77; H, 4.29; N, 3.15.

Acknowledgment. We gratefully acknowledge a grant from MEC-Spain CTQ2004-02201 and from Fundación Séneca (CARM) 02970/PI/05.

Supporting Information Available: General comments and computational details; NMR spectra; electrochemical, UV−vis, and UV−vis−NIR data; UV−vis and ^{1}H NMR titration data; cross-selectivity experiments; calculated structures, Cartesian coordinates, and energies for compounds **3′**, **5**, **6**, **7**, **9**, and **10′** and radical-cations **5**$^{\bullet+}$, **7**$^{\bullet+}$, and **11**$^{\bullet+}$; and MOs involved in MMCT for **5**$^{\bullet+}$ and **7**$^{\bullet+}$. This material is available free of charge via the Internet at http://pubs.acs.org.

OM700757M